Comparison of Stationarity Regions for Wireless Channels From 2 GHz to 30 GHz

(Invited Paper)

Yi Tan, Cheng-Xiang Wang
Institute of Sensors, Signals and Systems
School of Engineering & Physical Sciences
Heriot-Watt University, Edinburgh, UK.
Email: {yi.tan, cheng-xiang.wang}@hw.ac.uk

Jesper Ødum Nielsen, Gert F. Pedersen
APNet section, Dept. of Electronic Systems
Faculty of Engineering and Science
Aalborg University, Aalborg, Denmark
Email: {jni, gfp}@es.aau.dk

Abstract—Millimeter wave (mmWave) communication works in the frequencies above 6 gigahertz (GHz), with the system bandwidth up to 500 megahertz (MHz) or wider. In this case, the channel situations are dramatically different from the existing wireless channels in Third Generation/Fourth Generation (3G/4G) communication systems, and the stationarity of mmWave channels could be very different from our former knowledge. The focus of this paper is to study the frequency and spatial stationarities of mmWave channels. For better understanding, we compare the stationarity regions between mmWave channels and the channels below 6 GHz. First, the general average power delay profile (APDP) method is introduced as a metric to determine the size of the stationarity regions in time, frequency, and spatial domains. Then, the general APDP method is applied in the data analysis of a channel measurement. We find that the frequency stationarity regions of the channels are much larger in mmWave bands above 6 GHz than those in conventional bands below 6 GHz, while the spatial stationarity regions of the channels are much smaller in mmWave bands above 6 GHz than those in conventional bands below 6 GHz.

Keywords – mmWave channel, frequency/spatial stationarity region, general APDP method, correlation coefficient, allowance of similarity level (ASL).

I. INTRODUCTION

For the fifth generation (5G) wireless communication system, mmWave communication technology is one of the most promising candidates. The broad bandwidth resources in the mmWave frequency bands can allow the 5G system to greatly improve its capacity compared with the current 3G/4G networks. For example, about 7 GHz bandwidth resource in the 60 GHz band (unlicensed), and about 1 GHz bandwidth resource in the 28 GHz and 38 GHz bands are available [1]. As the study of communication channel is fundamental to the design of telecommunication systems, such dramatical changes of channel conditions could subvert our knowledge based on former studies of 3G/4G communications below 6 GHz. The smaller objects and the objects that are very close to each other may become very significant contributors to the propagation properties of mmWave channels.

The stationarity of a channel plays a fundamental role in channel modeling and data analysis of channel measurements, wide sense stationary (WSS) assumption is commonly used, and it has been widely accepted. In the standard channel mod-els, such as Wireless World Initiative New Radio (WINNER) II model [2], the concept of channel segments and drops has been used to represent the period of "quasi-stationarity" in time domain. In order to simulate the channels beyond the segments and drops, i.e., beyond the WSS condition, WINNER II has illustrated three ideas, which are used to describe the time-space evolution and scenarios transitions:

- Smooth transition between channel segments by power ramp-down and ramp-up of the clusters.
- Birth-death process. It is also used in European Cooperation in Science and Technology (COST) 2100 channel model [3].
- Using the temporal K-factor to describe the moving scatterers.

Regarding the frequency stationarity of the channel, the WINNER II model only considered that the path loss is frequency dependent. As to delay spread (DS), angle spread (AS), and Ricean K-factors, they do not show significant frequency dependence. They are therefore considered constant for each of the scenarios.

In the project Mobile and wireless communications Enablers for the Twenty-twenty Information Society (METIS), the frequency span of the mmWave channel models has been extended from 6 GHz to 100 GHz [4]. In [5], it was mentioned that the bandwidth used by mmWave communication systems could be up to 500 MHz or broader. In this case, the parameters, such as reflection, diffraction, diffusion, attenuation, blocking, and vegetation loss, etc. could be frequency dependent within such bandwidth, the assumption used in METIS and WINNER models that the channels are frequency stationarity may be violated in some circumstances.

MmWave communication will rely on beamforming technologies that are based on antenna arrays to compensate the high attenuation, and will probably use large antenna arrays. In recent research about massive multiple-input and multiple-output (Massive MIMO), the temporal and spatial non-stationarities were reported and modeled by a birth-death process [6]. In [7], it was reported that the spatial stationarity is very sensitive to the bandwidth of the mmWave channel. Therefore, the study in spatial stationarity could be very critical as well.

The study of stationarity is very important, since it is basic in channel estimation and modeling that we need to assume stationarity in order to achieve accurate channel parameter estimation. Further, new channel models for 5G should include the non-stationary properties. The contribution of this paper is trying to fill the gap, by comparing the stationarity properties in different frequency bands, it may offer a better way to understand the stationarity of mmWave channels. The rest of this paper is organized as follows. Section II introduces a general method to define the stationarity regions. Section III describes the mmWave channel measurement and the results of data analysis for the stationarity regions in frequency and spatial domains. Conclusions are finally drawn in Section IV.

II. STATIONARITY REGION IN TIME, FREQUENCY, AND SPATIAL DOMAINS

In the literature, the approach based on "sliding-window" correlation has been generally adopted to define the stationarity region. Examples are the covariance matrix distance (CMD) method [9]–[11] and the APDP method [12], etc. The principle is that the similarity of the channel properties could be represented by sliding-window correlation along the time, frequency or spatial axis. If the correlation coefficients are above a certain threshold, then the channel properties within that span of time, frequency or space have so high similarity that could be considered as statistically stationary. It means that it is inside of stationarity region, otherwise, outside of stationarity region. At the moment, most of the methods based on this approach were only developed to calculate the stationarity region in time and spatial domains. In this paper, a more general method based on APDP has been re-developed and extended to frequency domains. Though the CMD method could be used to calculate the stationarity region in the frequency domain, it must be based on multi-antenna transmitter and receiver. Compared with that, the general APDP method introduced does not have such limit.

A. Definition of Stationarity Region

Using the correlation-coefficient curve of the APDPs of the selected channel impulse responses, and if we determine an allowance of similarity level (ASL) of the channel properties as the threshold (between 0 to 1), then the region between the max of correlation coefficient to this ASL is considered statistical stationary, i.e. it satisfies the wide sense stationary uncorrelated scattering-homogeneous channels (WSSUS-HO) conditions and it is inside of the stationarity region.

There is no uniform verdict on the value of the threshold, i.e. ASL. It would depend on the situation how similar channel properties we require in post processing, the ASL need to be chosen carefully.

B. Time Domain general APDP Method

For a 1×1 wideband wireless channel, the instantaneous power delay profile (PDP) $P_h(t_i, \tau) = |h(t_i, \tau)|^2$ in specific time t_i can be seen as a snapshot of the channel. In Fig. 1, we assume there are N snapshots in total. We define $\overline{P_h}(t, \tau)$

as the average PDP of n-snapshots in one sliding window on the time axis t as

$$\overline{P_h}(t, \tau) = \frac{1}{n} \sum_{i=1}^{n} |h(t_i, \tau)|^2 \qquad (1)$$

and define another APDP $\overline{P_h}(t + \triangle t, \tau)$ of n-snapshots as it moves forward along the time axis t with a distance of $\triangle t$. The correlation coefficient between the APDPs is defined as

$$c(t, \triangle t) = \frac{\int \overline{P_h}(t, \tau)\overline{P_h}(t + \triangle t, \tau)d\tau}{\max\{\int \overline{P_h}(t, \tau)^2 d\tau, \int \overline{P_h}(t + \triangle t, \tau)^2 d\tau\}}. \qquad (2)$$

The stationary interval d_t is defined as the stationarity region in the time domain that the correlation coefficients $c(t, \triangle t)$ between the APDPs are all higher than the ASL c_{ASL}, i.e.

$$d_t = \max\{\triangle t|_{c(t,\triangle t) \geq c_{\text{ASL}}}\}. \qquad (3)$$

The n-snapshots used to calculate the APDPs are in a very small interval that we assume is much smaller than the stationary interval. Using the larger value of $\int \overline{P_h}(t, \tau)^2 d\tau$, and $\int \overline{P_h}(t + \triangle t, \tau)^2 d\tau$ in the denominator of (2) is to assure the correlation coefficient is smaller than 1. Note $\triangle t$ can be both positive and negative.

C. Spatial Domain general APDP Method

In spatial domain, for a $N \times 1$ wideband wireless channel scenario, the formulas to calculate the spatial stationarity regions are similar to the time domain case, with t replaced with r and $\triangle t$ replaced with $\triangle r$. Except the sliding windows are along spatial axis, i.e. along N antennas, the rest of procedures in the calculations are exactly the same.

D. Frequency Domain general APDP Method

The general APDP method in time and spatial domains are similar to the APDP method in [12]. In below, the general APDP method extends the APDP method to frequency domain, and it can be sorted in two situations:
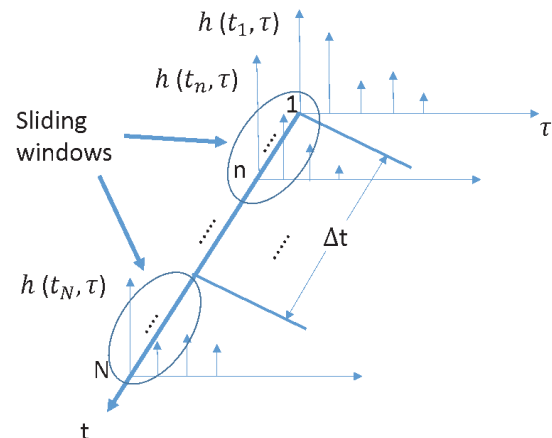
Fig. 1. Sliding-windows of the APDPs moving forward along the time axis.
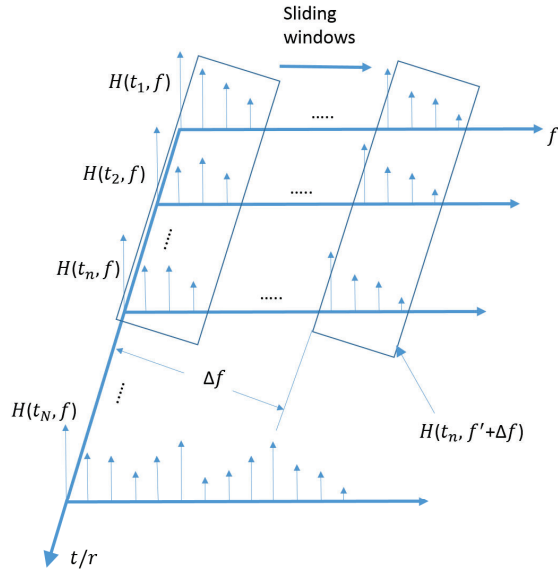
Fig. 2. Sliding-windows of the sub-APTFs moving forward along the frequency axis.

1) Case 1: Averaging on Snapshots: For a 1×1 wideband wireless channel, $P_H(t_t, f) = |H(t_i, f)|^2$ is the instantaneous power transfer function (PTF) of the channel for each snapshot at specific time t_i, and we assume there are N snapshots in total.

First, we average the power transfer functions of n-snapshots along time axis t as the average PTF (APTF), which can be expressed as

$$\overline{P_H}(t, f) = \frac{1}{n} \sum_{i=1}^{n} |H(t_i, f)|^2. \tag{4}$$

Second, as in Fig. 2, let us define $\overline{P_H}(t, f')$ as m-frequency-points sub-APTF in one sliding window on the frequency axis f, and define another m-frequency-points sub-APTF $\overline{P_H}(t, f' + \triangle f)$ as it moves forward along the frequency axis f with a distance of $\triangle f$. For avoiding the misunderstanding, we define f' as the frequencies within the sliding-windows. The correlation coefficient between the sub-APTFs is defined as

$$c(f', \triangle f) = \frac{\int \overline{P_H}(t, f') \overline{P_H}(t, f' + \triangle f) df'}{\max\{\int \overline{P_H}(t, f')^2 df', \int \overline{P_H}(t, f' + \triangle f)^2 df'\}}. \tag{5}$$

The stationary bandwidth d_f is defined as the physical stationarity region in the frequency domain that the correlation coefficients $c(f', \triangle f)$ between the sub-APTFs are all higher than the ASL c_{ASL}, i.e.

$$d_f = \max\{\triangle f|_{c(f', \triangle f) \geq c_{\text{ASL}}}\}. \tag{6}$$

The purpose of averaging on snapshots in (4) is to get a more stable spectrum, but requires that the channel is stationary in time domain. Likewise, we assume the sub-APTFs are smaller than stationary bandwidth in frequency domain, and

$\triangle f$ can be both positive and negative. Since $P_H(t, f)$ and $P_h(r, \tau)$ are Fourier transformation pairs in terms of "f" and "τ", we consider the calculation based on APTFs as a part of the general APDP method.

2) Case 2: Averaging on Antenna Array: Considering the use of a vector network analyzer (VNA) in the channel measurement, and that the channel is time-invariant, then only one snapshot of the channel is acquired per location. In a $N \times 1$ channel scenario, we can calculate PTF based on antenna arrays. Here we define $P_H(r_i, f) = |H(r_i, f)|^2$ as the PTF, and r_i is the antenna position along "r axis" in Fig. 2. Compare with the case 1, the APTF should be denoted as (7), and the first step now change to averaging the PTF on an antenna subarray instead, after that, the second step and the followings are the same

$$\overline{P_H}(r, f) = \frac{1}{n} \sum_{i=1}^{n} |H(r_i, f)|^2. \tag{7}$$

Similarly, the n-antenna subarray used to calculate the APTF should be selected within the stationary distance in spatial domain. The drawback of this case is the fluctuation of the results, because there may be only a few antenna elements to do the averaging within stationary distance.

III. MMWAVE CHANNEL MEASUREMENTS AND DATA ANALYSIS

A. MmWave Channel Measurement

The channel measurement providing the data to support this paper was performed in a basement environment, and is the same data used in [7], a big and almost empty room channel scenario. The measurement equipment consists of a VNA and a large virtual uniform circular array (UCA) with radius of 0.5 m. The frequency bands measured were in conventional frequency range of $2-4$ GHz, and mmWave frequency range of $14-16$ GHz and $28-30$ GHz, and there are 750 frequency points in each of the frequency bands (frequency interval is 2.67 MHz). The volume of the environment is 7.85 m $\times 7.71$ m, see Fig. 3. A Bi-Conical antenna with frequency range from $2-30$ GHz was used for both transmitter (Tx) and receiver (Rx), and the radiation pattern is omni-directional in the horizontal plane. The Bi-Conical antenna was fixed at about 1 m height at the Tx side, and for the Rx side, the Bi-Conical antenna was moving along the trajectory of the virtual UCA at 1 m height. The space between each two adjacent positions of the virtual UCA was 0.0044 m, which is less than $\lambda/2$ at 30 GHz. Both line-of-sight (LOS) and non-LOS (NLOS) measurements have been performed, using a metal board placed between Tx and Rx for the NLOS scenario. Fig. 4 illustrates how to use the virtual antennas within a sliding window to approximate the linear antenna array, and there are 16 virtual antennas in each sliding window.

B. Data Analysis

The channel measurement is a time-invariant $N \times 1$ channel scenario, and the frequency stationarity regions and spatial stationarity regions of the channels are our focus.
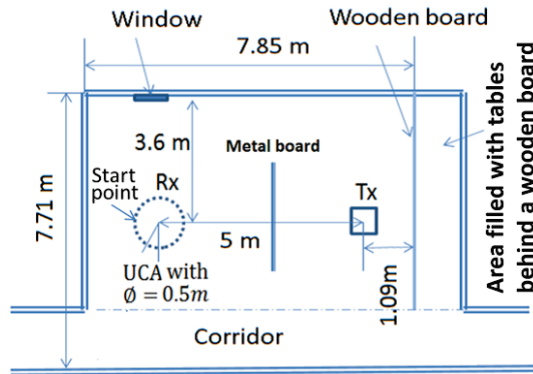
Fig. 3. Floorplan of channel measurements in the basement [7].
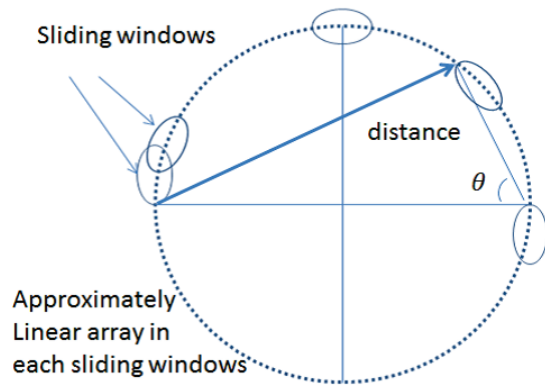
Fig. 4. Approximation of linear antenna subarrays [7].

1) Data Analysis of Frequency Stationarity Region: The calculation of frequency correlation coefficients is based on the case 2 of Frequency Domain general APDP Method: Averaging on Antenna Array. The results shown here are based on the averaging of virtual 16-antenna array consist of the first 16 virtual antennas from the UCA (720 virtual antenna). In order to reduce fluctuation in the results, the bandwidth of sub-APTFs in the sliding windows for each of the frequency bands is 5% of the center frequency. The calculation results are consistent with those obtained when using a narrower bandwidth, and 5% bandwidth is considered smaller than the frequency stationarity regions of each bands.

Fig. 5a represents the correlation coefficients vs. separation of sub-APTFs in number of $\triangle f$ in different frequency bands for the NLOS scenario. Given the ASL at 0.8, it is clear that the separation of sub-APTFs in 14−16 GHz and 28−30 GHz bands is larger than it is in 2−4 GHz band. The stationary bandwidth equals the number of $\triangle f$ times 2.67 MHz, therefore, the channels in 14−16 GHz and 28−30 GHz bands have larger stationary bandwidth, i.e. their stationarity regions are larger. Since the ASL could also be other values, in Fig. 5b, we illustrate the stationary bandwidths of those three bands for each of the ASLs from 0.4 to 0.95, and it shows that the stationarity regions in 14−16 GHz and 28−30 GHz bands are much larger than it is in 2−4 GHz band. The

above results are for a single location of the virtual array, we have calculated the frequency stationarity regions based on other virtual 16-antenna arrays around the whole UCA, the results between the 14–16 GHz band and 28–30 GHz band are comparable. The calculations based on some virtual 16-antenna arrays show larger frequency stationarity regions in 14–16 GHz band, but some with larger frequency stationarity regions in 28–30 GHz bands. However, all of them show much larger frequency stationarity regions in mmWave frequency bands than it is in 2–4 GHz band.

In Fig. 6, the LOS scenario, it is difficult to find a proper ASL to determine which one has larger stationary bandwidth between the frequency bands at 14−16 GHz and 28−30 GHz, since they have very similar correlation coefficients at very high values. The reason could be the attenuation increases dramatically as the frequency goes higher, and the LOS components become more dominant in the results. In the data processing, the Space-Alternating Generalized Expectation maximization (SAGE) algorithm [8] has been used to estimate the multi-path components (MPCs). The condensed parameters are found in table I for the NLOS scenario. As we expected, the ratio of LOS component over NLOS components, i.e. K factor in [13], is 3.3 dB at 2−4 GHz band, 12.7 dB at 14−16 GHz band, and 15 dB at 28−30 GHz band. Since the NLOS components are the results of the inter-actions with the channel environment, NLOS components reflect the properties of channel environment. It makes sense that for the channels at 14−16 GHz and 28−30 GHz frequency bands, the received power of NLOS components are much weaker than that of the LOS component, and the correlation coefficients mainly reflect the LOS component itself.

WINNER II channel models support 100 MHz system bandwidth, which is considered within the frequency stationarity region. The frequency stationarity region found in this work, which is 18.69 MHz for the 2−4 GHz band on the level ASL at 0.5, much smaller. One reason could be that the ASL is chosen too high. Another reason could be the size of the scatterers in the empty room is closer to the wavelength of the frequencies in 2−4 GHz bands, such as wall, ceiling, and windows, etc., those frequencies are very sensitive in this scenario. We can also observe that the correlation coefficients of sub-APTFs in 2−4 GHz band are all higher than 0.3 for the distance of sub-APTFs within $175 \times \triangle f$ (467.25 MHz) in Fig. 5a. Though this bandwidth seems too large, but for this specific scenario, it could be a reasonable size of frequency stationarity region for 2−4 GHz band.

2) Data Analysis of Spatial Stationarity Region: Fig. 7a, represents the correlation coefficients vs. distance of subarrays

Table I. Estimated parameters in the NLOS scenario.

Bands (GHz)	Mean delay (ns)	DS (ns)	Mean angle (°)	AS (°)
2-4	36.60	11.67	89.72	3.345
12-14	37.49	9.76	82.89	19.05
28-30	33.50	7.7	102.08	43.56

650
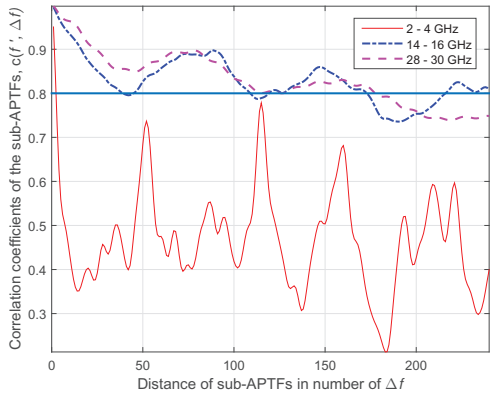
(a)
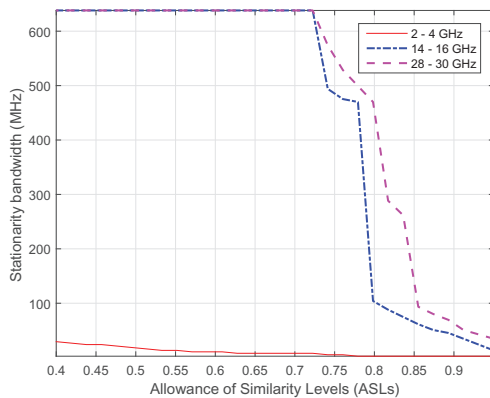
(b)

Fig. 5. Frequency stationarity regions in the NLOS scenario: (a) correlation coefficients vs. separation of sub-APTFs in number of $\triangle f$, and (b) stationary Bandwidth vs. ASLs.

in number of $\triangle r$ in different frequency bands for the NLOS case. We can see that the correlation coefficients are clearly separated for ASLs below 0.72, and we can find that the stationary distance is largest in the $2-4$ GHz band, and smallest in the $28-30$ GHz band. Fig. 7b illustrates the stationary distance (in meter) of those three bands for each of the ASLs from 0.4 to 0.95. It shows that the spatial stationarity regions are much smaller in 14–16 GHz, 28–30 GHz bands than it is in 2–4 GHz band. This is reasonable, since as the frequency goes higher, the contribution of the channel properties by small objects become more significant, and the angle of arrival (AoA) of the MPCs become more sensitive. The AS in table I also explains that larger AS implies smaller

Table II. Frequency stationarity regions in the NLOS scenario.

Bands (GHz)	Size of region for ASL @ 0.5 (MHz)	Size of region for ASL @ 0.8 (MHz)
2-4	18.69	2.67
12-14	638.13	104.13
28-30	638.13	285.29

span of stationarity region, which is based on HO in [13].

However, we could observe that in Fig. 7a, the stationary distance in the $2-4$ GHz band is very close to that in $14-16$ GHz band for the ASLs above 0.72, the reason is unknown yet. For LOS case in Fig. 8, the correlation coefficients of those three bands looks very similar for the ASL down to 0.6. For the ASLs below 0.6, the stationarity region in $2-4$ GHz band become larger than those in $14-16$ GHz and $28-30$ GHz bands, but the difference of correlation coefficients between the frequency bands at $14-16$ GHz and $28-30$ GHz is very small. Again, the reason is likely that the LOS component is dominant, and the correlation coefficients only reflect the LOS component itself.

The size of spatial stationarity region can be considered as decorrelation distance of large scale fading, the threshold suggested is e^{-1} (about 0.367) in [14]. In METIS models, the decorrelation distance in mmWave range is about a few meters, and in below 6 GHz bands, it is about a few tens of meters [4]. Due to the fact that as the signal bandwidth becomes broader, the spatial stationarity region become smaller [7], and since the bandwidth of channels in the data analysis is 2 GHz, the size of the spatial stationarity regions shown are reasonable.

IV. CONCLUSIONS

In this paper, the general APDP method has been extended to time, frequency, and spatial domains to determine the stationarity regions of the wireless channels. It is not constrained by frequency, channel scenarios, or number of antennas used in the transmitter and receiver. We have applied the general APDP method to the data processing of a channel measurement, which contains three different bands that are in the conventional frequency range of $2-4$ GHz and mmWave frequency range of $14-16$ GHz and $28-30$ GHz. The comparison of the stationarity regions based on the correlation coefficients of the APDPs have been studied. We have found that the frequency stationarity regions of the channels in mmWave frequency range are much larger than those in the conventional frequency range, while the spatial stationarity

Fig. 6. Frequency stationarity regions in the LOS scenario.

(a)
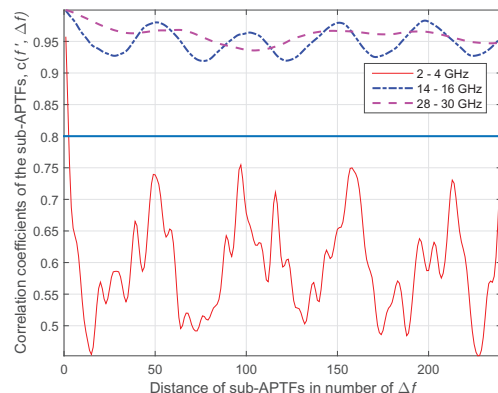
Fig. 8. Spatial stationarity regions in the LOS scenario.
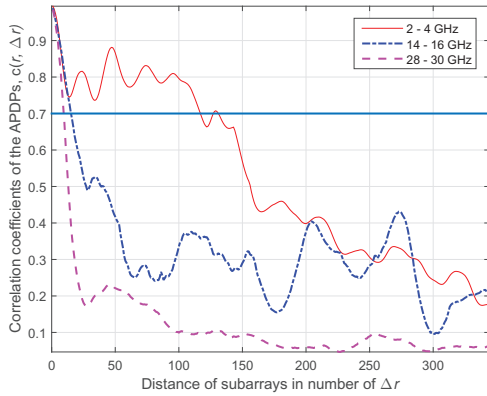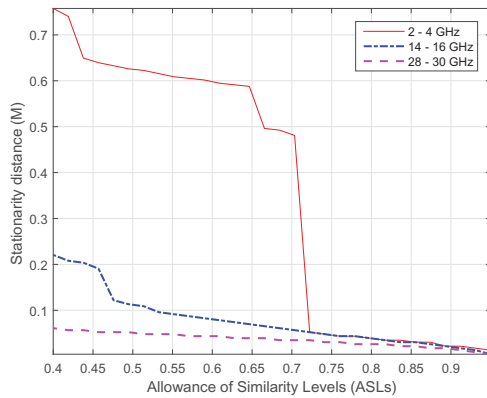
(b)

Fig. 7. Spatial stationarity regions in the NLOS scenario: (a) correlation coefficients vs. distance of subarrays in number of $\triangle r$, and (b) stationary distance vs. ASLs.

regions of the channels in mmWave frequency range are much smaller than those in the conventional frequency range.

ACKNOWLEDGMENT

REFERENCES

[1] A. F. Molisch and F.Tufvesson, "Propagation channel models for next-Generation wireless communications systems," *IEICE Trans. Commun.*, vol. E97-B, no.10, pp. 2022–2034, Oct. 2014.

[2] K. Pekka, J. Meinil, L. Hentil, X. Zhao, T. Jms, C. Schneider, and M. Narandzic et al., "WINNER II channel models," D1.1.2 V1.2, IST-4-027756 WINNER II Deliverable, 4 Feb. 2008.
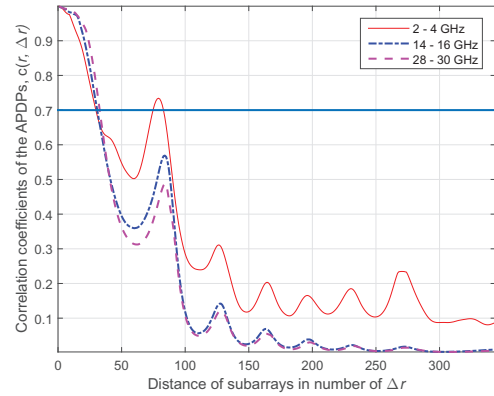
[3] R.Verdone and A. Zanella, *Pervasive Mobile and Ambient Wireless Communications: COST Action 2100.* Springer Science & Business Media, 2012.

[4] V. Nurmela, et al., "METIS Channel Models," ICT-317669-METIS, Deliverable D1.4, Feb. 2015.

[5] W. Rohl, et al., "Millimeter-wave beamforming as an enabling technology for 5G cellular communications: theoretical feasibility and prototype results," *IEEE Commun. Mag.*, vol. 52, no. 2, pp. 106–113, Feb. 2014.

[6] S. Wu, C.-X. Wang, H. Haas, H. Aggoune, M. M. Alwakeel, and B. Ai, "A non-stationary wideband channel model for massive MIMO communication systems," *IEEE Trans. Wireless Commun.*, vol. 14, no. 3, pp. 1434–1446, Mar. 2015.

[7] Y. Tan, J. Ø. Nielsen, and G. Pedersen, "Spatial stationarity of ultrawideband and millimeter wave radio channels," *Int J Antennas Propag.*, vol. 2016, Article ID 3212864, 7 pages, 2016.

[8] B. H. Fleury, M. Tschudin, R. Heddergott, D. Dahlhaus, and K. Ingeman Pedersen, "Channel parameter estimation in mobile radio environments using the SAGE algorithm," *IEEE J. Sel. Areas Commun.*, vol. 17, no. 3, pp. 434–450, Mar. 1999.

[9] M. Herdin and E. Bonek, "A MIMO correlation matrix based metric for characterizing non-stationarity," in *Proc. IST Mobile Wireless Commun. Summit*, Lyon, France, Jun. 2004, 5 pages.

[10] M. Herdin, N. Czink, H. Ozcelik, and E. Bonek, "Correlation matrix distance, a meaningful measure for evaluation of non-stationary MIMO channels," in *Proc. IEEE Veh. Technol. Conf. (VTC '05-Spring)*, Stockholm, Sweden, Jan. 2005, vol. 1, pp. 136–140.

[11] O. Renaudin, V. Kolmonen, P. Vainikainen, and C. Oestges, "Impact of correlation matrix estimation accuracy on the computation of stationarity intervals," in *Proc. Eur. Conf. Antennas Propag. (EuCAP '10)*, Barcelona, Spain, Apr. 2010, pp. 1–5.

[12] A. Gehring, M. Steinbauer, I. Gaspard, and M. Grigat, "Empirical channel stationarity in urban environments," in *Proc. Eur. Personal Mobile Communications Conf. (EPMCC'01)*, Vienna, Austria, Feb. 2001.

[13] A. Paulraj, R. Nabar, and D. Gore, *Introduction to space-time wireless communications.* Cambridge university press, 2003.

[14] M. Zhu, F. Tufvesson, and J. Medbo, "Correlation properties of large scale parameters from 2.66 GHz multi-site macro cell measurements," in *Proc. IEEE Veh. Technol. Conf. (VTC '11-Spring)*, Budapest, Hungary, May 2011, pp. 1–5.